Unsteady MHD Flow of Casson Fluid Past Vertical Surface Using Laplace Transform Solution

Article *in* Journal of Computational Biophysics and Chemistry · January 2023

DOI: 10.1142/S2737416523400100

CITATION
1

READS
202

5 authors, including:

Farhan Ali
وفاقی اردو یونیورسٹی (وفاقی جامعہ اردو
52 PUBLICATIONS **718** CITATIONS
SEE PROFILE

Aurang Zaib
Federal Urdu University of Arts, Science and Technology
159 PUBLICATIONS **2,744** CITATIONS
SEE PROFILE

Muhammad Khalid
Federal Urdu University of Arts, Science and Technology
77 PUBLICATIONS **454** CITATIONS
SEE PROFILE

B. Hemalatha
Rajalakshmi Institute of Technology
14 PUBLICATIONS **48** CITATIONS
SEE PROFILE

Journal of Computational Biophysics and Chemistry

Research

Cite This: *J. Comput. Biophys. Chem.* **2023**, *22* (3), 361–370

Unsteady MHD Flow of Casson Fluid Past Vertical Surface Using Laplace Transform Solution

Farhan Ali*, A. Zaib and M. Khalid

Department of Mathematical Sciences, Federal Urdu University of Arts, Science and Technology Gulshan-e-Iqbal, University Road, Karachi 75850, Pakistan

T. Padmavathi

Department of Mathematics, Saveetha Engineering College, Chennai 602105, India

padmavathit@saveetha.ac.in

B. Hemalatha

Department of Mathematics, VISTAS-Vels University, Pallavaram, Chennai 600117, India

*Corresponding author. Email: *farhanali@fuuast.edu.pk*

ABSTRACT: The study explores the velocity of Casson fluid that is time-independent over an exponentially infinite isotherm vertical permeable sheet. The impact of magnetohydrodynamic (MHD) with Casson flow over the permeability sheet is examined. In contrast, thermal radiation and heat sink parameters have been incorporated. This study's primary goal is to determine the significance of thermal radiation on Casson flow with MHD using an analytical solution over a permeable sheet. The flow of the fluid occurs above the sheet when y is greater than zero, and the sheet extends far away in the x-direction. The model of governing equations is reduced by applying a suitable set of dimensionless parameters. These dimensionless systems of equations are solved through the Laplace transformation method. The impacts of various variables over velocity, temperature, concentration, skin friction, and Nuseelt number are scrutinized. These variables contain magnetic field M, Casson fluid parameter β, Ghroshof number Gr, modified Grashof number Gc, Prandtl number Pr, thermal radiation Rd and Scimdth number Sc. These plots are sketched for the considerable magnitude of these variables through the Mathematica Software, and these plots are discussed in detail. Results show that the increasing value of M reduces the fluid velocity but velocity of fluid is enhanced with larger values of Gr, Gc and β. The impact of Skin friction and Nusselt number is elaborated by tabular outlined.

KEYWORDS: Laplace; MHD; Casson fluid; permeable sheet; incompressible.

NOMENCLATURE

α	Thermal diffusivity (m^-2s^-1)
β	Casson fluid parameter (Dimensionless)
η	Similarity parameter (Dimensionless)
μ	Coefficient of viscosity ($Ra.s$)
ν	Kinematic viscosity (m^2s^-1)
ϕ	Dimensionless concentration (Dimensionless)
ρ	Density of the fluid (kgm^-3)
σ^2	Porosity number
θ	Dimensionless temperature (Dimensionless)
$beta^*$	Coordinate normal to the plate (m^-2s^-1)
c_p	Specific heat ($J.kg^-1K$)
$erfc$	Complementary error function
g	Acceleration due to gravity (m^2s^-2)
Gc	Modified Ghroshof number (Dimensionless)
Gr	Ghroshof number (Dimensionless)
K	Thermal conductivity (Wm^-1s^-2)
M	Magnetic number (Dimensionless)

Received: 22 December 2022
Accepted: 3 January 2023
Published: 18 February 2023

DOI: 10.1142/S2737416523400100
J. Comput. Biophys. Chem. **2023**, *22* (3), 361–370

Pr	Prandtl number (Dimensionless)
Sc	Schmidt number (Dimensionless)
t	Dimensionless time (Dimensionless)
U	Dimensionless velocity (Dimensionless)

1. INTRODUCTION

The Casson fluid is considered a non-Newtonian fluid due to its rheological properties. This classification is based on the relationship between shear stress and shear rate. At low shear strains, it exhibits yield stress behavior, but as the shear strain reaches a critical value, it changes to the behavior of a Newtonian fluid. A liquid with shear thinning properties is considered to have a zero shear rate at infinite thickness, yields less stress when there is no flow, and a zero thickness at an infinite rate of shear. *Some current developments on non-Newtonian fluid with geometries were cited in Refs.* 1–7. Mustafa *et al.*[8] discussed the Casson fluid approaching the boundary layer flow over a semi-infinite plate. Bhattacharyya[9] considered the magnetohydrodynamic (MHD) flow of Casson fluid in the influence of thermal radiation over-stretching sheets. Mukhopadhyay *et al.*[10] examined the time-dependent flow of Casson fluid over a stretching sheet. Nadeem *et al.*[11] investigated Casson fluid's MHD boundary layer flow over an exponentially permeable shrinking sheet. Vijay *et al.*[12] studied the combined effect of thermal and chemical reactions on MHD Casson fluid. Santoshi *et al.*[13] probed on MHD Casson flow over a vertical sheet in varying viscosities and heat sources.

The significance of MHD is in agriculture, geophysics, astrophysics, and the petroleum sector. The important mechanism for investigating the geological development, plasma confinement, MHD generators, nuclear reactor cooling, and many more. MHD has more applications in the field of metrology and aeronautics. Using the perturbation approach, Gupta *et al.*[14] described the free convection flow across linearly vertically accelerated plates under viscous dissipative. Muthucumaraswamy *et al.*[15] conducted a precise analysis of MHD unsteady flow across an accelerating plate, including heat and mass transport. Kafousias and Raptis[16] extended the study of Muthucumaraswamy *et al.*,[15] including the mass transfer effect with suction and injection. Raptis and Singh[17] explored the flow over an infinite vertical plate by the addition impulse and accelerated plate motion. Force convection affects flow over a vertically accelerated plate under the MHD effect with variable suction and heat flux. The MHD flow on heat and mass transfer with mixed connectives under the Soret and Dufour effect was explored by Dhanalakshmi *et al.*[18] Investigating the function of MHD flow in the porous surface was carried out by Kallepalli *et al.*[19] The impact of thermal radiation on MHD fluid flow over a semi-infinite flat plate was considered by Dharmaiah *et al.*[20]

The MHD and viscous fluid were established by Sivaiah *et al.*[21] by analyzing permeable channel MHD flow. The MHD micropolar fluid was studied by Reddy *et al.*[22] under the influence of Soret and Dufour. The influence of MHD was developed by Sujatha *et al.*[23] due to cone and concave surfaces with chemical interaction. Ibrahim *et al.*[24] assumed that the MHD flow across a vertical surface triggered the chemical reaction chemical reaction. The time-dependent mixed convective flow on micropolar fluid caused by a porous conduit was described by Kumar *et al.*[25] The primary purpose of this body of work is to investigate how the velocity of Casson fluid's transient flow changes under the effect of a variety of embedded characteristics. Padmavathi *et al.*[26–30] established various respiratory tract fluid flows due to forced and free convection stream inaugurating a new vision of lung mechanism under the impact of chemical reaction and heat absorption along with MHD and the effects of porosity.

The prime idea of this study is to examine the role of hear and mass transfer of Casson fluid in the presence of numerous variables with MHD and Permeable effect. *In this manner, the purpose of this work was to perform an investigation into the fluid dynamic impacts of thermal in an unstable mucus fluid flowing conductivity on flow characteristics through an isothermal channel.* By using a suitable set of dimensionless variables, the model's governing equations, along with the initial and boundary conditions, are transformed into a form without dimensions. The Laplace Transformation can be used to find analytical answers for figuring out the Casson fluid's velocity distribution, temperature profile and concentration field. The answers are expressed in terms of the complementary and exponential error functions. With the help of the MATHEMATICA software, we present graphs to show how different factors affect velocity, temperature, and concentration.

DOI: 10.1142/S2737416523400100
J. Comput. Biophys. Chem. **2023**, *22* (3), 361–370

2. MODEL FORMULATION

Let us investigate the incompressible transient flow of the MHD Casson fluid model with thermal radiation and heat source above an accelerating porous plate. First, it is demonstrated that the form of the fluid's velocity field is taken into account. In addition, the magnetic field of strength considered along the x-axis and y-axis is taken opposite the x-axis. Further, at $t = 0$, the velocity of the porous channel is $U = e^{at}$ is shown in Fig. 1. In light of the observations mentioned above for the Boussinesq's approximation, the unsteady flow is governed by the following equations.[26]

Continuity equation

$$\frac{\partial v}{\partial y} = 0. \tag{1}$$

Momentum equation

$$\frac{\partial u}{\partial t^*} = g\beta'(T - T_\infty) + g\beta^*(C - C_\infty) + \nu\left(1 + \frac{1}{\beta}\right)\frac{\partial^2 u}{\partial y^2} - \frac{\sigma B_\circ^2}{\rho}u. \tag{2}$$

Energy equation

$$\rho C_p \frac{\partial T}{\partial t^*} = k\frac{\partial^2 T}{\partial y^2} - Q_\circ(T - T_\infty) - \frac{\partial q_r}{\partial y}. \tag{3}$$

Concentration equation

$$\frac{\partial C}{\partial t^*} = D\frac{\partial^2 C}{\partial y^2}. \tag{4}$$

Here, u and v are the velocity components in the direction of x and y. The coefficient of volumetric expansion with temperature is β', the coefficient of volumetric expansion with temperature is β_t, kinematic viscosity is ν, the temperature of the fluid is T, ambient temperature is T_∞, the concentration of the fluid is C, ambient concentration is C_∞, electrical conductivity is σ, the density of the fluid is ρ, specific heat is C_p, magnetic field is $B_\circ$ and t denotes the time. The boundary conditions are

$$\left.\begin{array}{llll} u = 0, & T = T_\infty, & C = C_\infty & \text{for all } y \text{ and } t^* \le 0, \\ u = u_\circ, & T = T_w, & C = C_w & \text{at } y = 0, \\ u = 0, & T = T_w, & C = C_w & \text{at } y \to 0. \end{array}\right\} \tag{5}$$

The local gradient is given by

$$\frac{\partial q_r}{\partial y} = -4b\sigma(T_\infty^4 - T_\infty). \tag{6}$$

This is achieved by building on a Taylor's expansion while disregarding higher-order terms

$$T^4 \cong 4T_\infty^3 T - 3T_\infty^4. \tag{7}$$

By using Eqs. (5) and (6), Eq. (2) becomes

$$\rho C_p \frac{\partial T}{\partial t} = k\frac{\partial^2 T}{\partial y^2} - Q_\circ(T - T_\infty) + 16\sigma b^* T_\infty^3(T - T_\infty), \tag{8}$$

where we introduce the dimensionless variable as

$$\left.\begin{array}{llllll} U = \dfrac{u}{u_\circ}, & \chi = \dfrac{x'}{h}, & t = \dfrac{t'u_\circ^2}{\nu}, & Y = \dfrac{yu_\circ}{\nu}, & \mathrm{Sc} = \dfrac{\nu}{D}, \\ \theta = \dfrac{T - T_\infty}{T - T_w}, & \mathrm{Rd} = \dfrac{16\sigma b^* \nu^2 T_\infty^3}{ku_\circ^2}, & \mathrm{Gc} = \dfrac{g\nu\beta'(C_w - C_\infty)}{u_\circ^3}, & & \\ \mathrm{Gr} = \dfrac{g\nu\beta^*(T_w - T_\infty)}{u_\circ^3}, & \mathrm{Pr} = \dfrac{\rho\nu C_p}{k}, & \phi = \dfrac{C - C_\infty}{C_w - C_\infty}. & & \end{array}\right\} \tag{9}$$

Equations (2), (4) and (8) become

$$\frac{\partial u}{\partial t} = \left(1 + \frac{1}{\beta}\right)\frac{\partial^2 u}{\partial y^2} + \mathrm{Gr}\theta + \mathrm{Gc}\phi - Mu, \tag{10}$$

$$\frac{\partial \theta}{\partial t} = \frac{1}{\mathrm{Pr}}\frac{\partial^2 u}{\partial \theta^2} - \mathrm{Rd}\theta - Q\theta, \tag{11}$$

$$\frac{\partial \phi}{\partial t} = \frac{1}{\mathrm{Pr}}\frac{\partial^2 \phi}{\partial y^2}. \tag{12}$$

Here, magnetic field ($M = \frac{\sigma\mu B_\circ^2}{U_\circ^2}$), mass Grashof number ($\mathrm{Gr} = \frac{g\nu\beta'(C_w - C_\infty)}{u_\circ^3}$), Grashof number ($\mathrm{Gr} = \frac{g\nu\beta^*(T_W - T_\infty)}{u_\circ^3}$), Prandtl number ($\mathrm{Pr} = \frac{\mu C_p}{k}$), Schmidt number ($\mathrm{Sc} = \frac{\nu}{D}$). The boundary conditions are

$$\left.\begin{array}{llll} U = 0, & \theta = 0, & \phi = 0 & \text{for all } Y \text{ and } t \le 0, \\ U = e^{at}, & \theta = 1, & \phi = t & \text{at } Y = 0, \\ U \to 0, & \theta \to 0, & \phi \to 0 & \text{at } Y \to \infty. \end{array}\right\} \tag{13}$$

We obtain the solution of a nondimensional Eqs. (10)–(12) with boundary condition by applying the Laplace

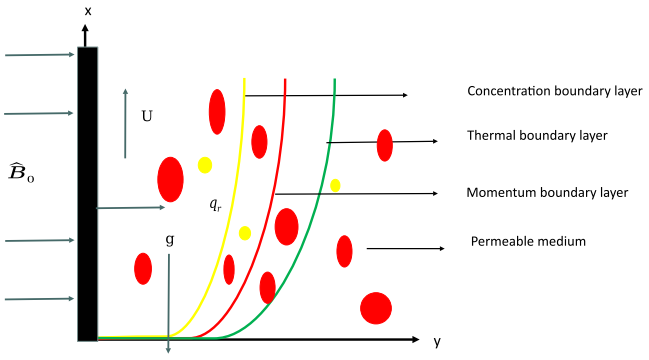

Fig. 1. (Color online) A flow model.

DOI: 10.1142/S2737416523400100
J. Comput. Biophys. Chem. **2023**, *22* (3), 361–370

transformation technique in relation to t (time) to the preceding equations, the resulting equations are

$$L(u) = \mathrm{Gr}\epsilon_1\left(e^{\frac{-Y\sqrt{s+M}}{\beta}}\right) + \mathrm{Gr}\epsilon_1\left(\frac{e^{-Y\sqrt{\mathrm{Pr}(s+\alpha)}}}{\epsilon^2(s+\epsilon)}\right) - \mathrm{Gr}\epsilon_1\left(\frac{e^{-Y\sqrt{\mathrm{Pr}(s+\alpha)}}}{\epsilon^2 s}\right) + \mathrm{Gr}\epsilon_1\left(\frac{e^{-Y\sqrt{\mathrm{Pr}(s+\alpha)}}}{\epsilon s^2}\right) + \frac{\mathrm{Gc}}{S^3(\mathrm{Sc}-1)}\left(e^{\frac{-Y\sqrt{S+M}}{\beta}} - e^{-Y\sqrt{\mathrm{Sc}s}}\right), \quad (14)$$

$$L(\theta) = \frac{e^{-Y\sqrt{\mathrm{Pr}(s+\alpha)}}}{s^2}, \quad (15)$$

$$L(\phi) = \frac{e^{-Y\sqrt{\mathrm{Sc}s}}}{s^2}. \quad (16)$$

Following the inverse Laplace-transform method, the governing Eqs. (14)–(16) are solved, the solutions are deduced as follows.

$$\begin{aligned}U = {} & \frac{e^{at}}{2}(e^{-Y\sqrt{a+M}}\mathrm{erfc}(\eta - \sqrt{a+M}) \\ & + e^{Y\sqrt{a+M}}\mathrm{erfc}(\eta + \sqrt{a+M})) \\ & + \mathrm{Gr}\epsilon_1(e^{-Y\sqrt{M}}\mathrm{erfc}(\eta - \sqrt{M}) \\ & + e^{Y\sqrt{M}}\mathrm{erfc}(\eta + \sqrt{M})) \\ & + \frac{\mathrm{Gr}\epsilon_1}{\epsilon^2}(e^{-Y\sqrt{\mathrm{Pr}(\epsilon+a)}}\mathrm{erfc}(\eta - \sqrt{\mathrm{Pr}(\epsilon+a)}) \\ & + e^{Y\sqrt{\mathrm{Pr}(\epsilon+a)}}\mathrm{erfc}(\eta + \sqrt{\mathrm{Pr}(\epsilon+a)})) \\ & + \frac{\mathrm{Gr}\epsilon_1}{2\epsilon^2}(-e^{-Y\sqrt{\mathrm{Pr}\alpha}}\mathrm{erfc}(\sqrt{\mathrm{Pr}\eta} + 2\sqrt{t\alpha}) \\ & + -e^{2Y\sqrt{\mathrm{Pr}\alpha}}\mathrm{erfc}(\sqrt{\mathrm{Pr}\eta} - 2\sqrt{t\alpha})) \\ & + \frac{\mathrm{Gr}\epsilon_1}{4\epsilon\sqrt{\alpha}}(e^{-Y\sqrt{\mathrm{Pr}\alpha}}(-Y\sqrt{\mathrm{Pr}} + 2t\sqrt{\alpha}) \\ & \times \mathrm{erfc}(\eta\sqrt{\mathrm{Pr}} + 2\sqrt{t\alpha})) \\ & + e^{2Y\sqrt{\mathrm{Pr}\alpha}}(Y\sqrt{\mathrm{Pr}} + 2t\sqrt{\alpha})\mathrm{erfc}(\eta\sqrt{\mathrm{Pr}} + 2\sqrt{t\alpha})) \\ & + \frac{\mathrm{Gc}}{s^3(\mathrm{Sc}-1)}\left(\frac{1}{16M^{3/2}\sqrt{\pi}}e^{-\frac{(2t\sqrt{M}+Y)^2}{4t}}\right. \\ & \times (\sqrt{\pi}e^{Mt+\eta^2}(4t^2M^{3/2} + Y - 4MtY) \\ & + \sqrt{\pi}e^{Mt+2Y\sqrt{M}+\eta^2}(4M^{3/2}t^2\sqrt{M}Y^2) \\ & \left. - 4Y\sqrt{Mt}e^{\sqrt{M}Y})\right) \\ & + \frac{\mathrm{Gc}}{s^3(\mathrm{Sc}-1)}(e^{Mt+\eta^2}(4M^{3/2}t^2 + Y - 4MtY \\ & + Y^2\sqrt{M})\mathrm{erfc}(2\sqrt{Mt} - \eta)) \\ & - \frac{\mathrm{Gc}}{s^3(\mathrm{Sc}-1)}(e^{Mt+2Y\sqrt{M}+\eta^2}\sqrt{\pi}(4M^{3/2}t^2 - Y \\ & + 4MtY + Y^2\sqrt{M})\mathrm{erfc}(2\sqrt{Mt} + \eta)) \\ & + \frac{\mathrm{Gc}}{s^2(\mathrm{Sc}-1)}\left(-\frac{2e^{-Sc\eta^2}\sqrt{\mathrm{Sc}t}Y(10t + \mathrm{Sc}Y^2)}{24\sqrt{\pi}}\right. \\ & \left. + (12t^2 + 12\mathrm{Sc}tY^2 + \mathrm{Sc}^2Y^4)\mathrm{erfc}(\sqrt{\mathrm{Sc}}\eta)\right), \end{aligned} \quad (17)$$

$$\begin{aligned}\theta = {} & \frac{t}{2}\left(e^{-\sqrt{\mathrm{Pr}\alpha}}\mathrm{erfc}(\sqrt{\mathrm{Pr}}\eta - \sqrt{\mathrm{Pr}\alpha})\right. \\ & + e^{\sqrt{\mathrm{Pr}\alpha}}\mathrm{erfc}(\sqrt{\mathrm{Pr}}\eta + \sqrt{\mathrm{Pr}\alpha}) \\ & - \frac{Y}{2\sqrt{b\mathrm{Pr}}}(e^{\sqrt{\mathrm{Pr}\alpha}}\mathrm{erfc}(\sqrt{\mathrm{Pr}}\eta - \sqrt{\mathrm{Pr}\alpha}) \\ & \left. + e^{\sqrt{\mathrm{Pr}\alpha}}\mathrm{erfc}(\sqrt{\mathrm{Pr}}\eta + \sqrt{\mathrm{Pr}\alpha}))\right), \end{aligned} \quad (18)$$

$$\phi = t\left((1 + 2\eta^2\mathrm{Sc})\mathrm{erfc}(\eta\sqrt{\mathrm{Sc}}) - 2\eta\sqrt{\frac{\mathrm{Sc}}{\pi}}e^{-\eta^2\mathrm{Sc}}\right). \quad (19)$$

3. RESULT AND DISCUSSION

The Laplace transform method is utilized to solve the equations describing the flow to provide exact analytical solutions for the velocity, temperature, and

Table 1. Shows fluctuation in the skin friction.

M	Gr	Gc	β	t	Skin Friction
0.5	1	1	1	0.2	1.3047
0.6					1.3138
0.7					1.325
0.8					1.337
0.9					1.3494
	1.1				1.5104
	1.2				1.6713
	1.3				1.8323
	1.4				1.9933
	1.5				2.1543
		0.1			2.3886
		0.2			2.3626
		0.3			2.3365
		0.4			2.3104
		0.5			2.2846
			1.1		2.2374
			1.2		2.1773
			1.3		2.1017
			1.4		2.0079
			1.5		1.8929
				0.3	0.9581
				0.4	0.5918
				0.5	0.413
				0.6	0.2758
				0.7	0.1453

Table 2. Shows fluctuation in the Nusselt number.

Rd	Q	Pr	b	Nusselt Number
0.1	0.1	1	0.1	0.8507
0.2				1.128
0.3				1.3871
0.4				1.6346
0.5				1.874
	0.2			2.1075
	0.3			2.3364
	0.4			2.5619
	0.5			2.7847
	0.6			3.0056
		1.1		3.0958
		1.2		3.1832
		1.3		3.2685
		1.4		3.352
		1.5		3.4341
			0.3	6.2697
			0.4	5.4298
			0.5	4.8565
			0.6	4.4334
			0.7	4.1045

concentration. In addition, graphical analysis was performed to determine how different physical characteristics affected the flow of fluid. Tables 1–3 were used to highlight the variations in skin friction, Nusselt number, and Sherwood number that occurred due to differences in physical factors.

Figure 2 shows the effect of magnetic field M on fluid velocity. As the magnetic field parameter M increases, as seen in Fig. 2, the speed declines. Physically, the momentum barrier layer often thins when a magnetic field is applied to a fluid flow capable of conduction. The cause of this is that Lorentz forces, which are resistance forces produced during this process and have a detrimental effect on fluid flow, are created. Figure 3 displays the impact of Gr and Gc over fluid velocity. The more significant values of Gr and Gc enhance the fluid velocity. Figure 4 sketched the effect of the Casson parameter β over fluid velocity. We observe that when the value grows β, the speed and the viscous flow diminish. Therefore, the velocity magnitude is more significant in Casson fluid than in viscous fluids since the Casson fluid is less dense.

Figure 5 represents the fluctuation of time t over fluid velocity. When the time is increased, the momentum boundary layer is also grown, which leads to an increase in the fluid speed being observed. It is possible to see the opposite finding on the temperature

Table 3. Shows fluctuation in the Sherwood number.

Sc	t	Sherwood Number
1.0		0.1128
1.1		0.1183
1.2		0.1236
1.3		0.1286
1.4		0.1335
1.5		0.1381
	0.2	0.2763
	0.3	0.4145
	0.4	0.5527
	0.5	0.6909
	0.6	0.8291
	0.7	0.9673

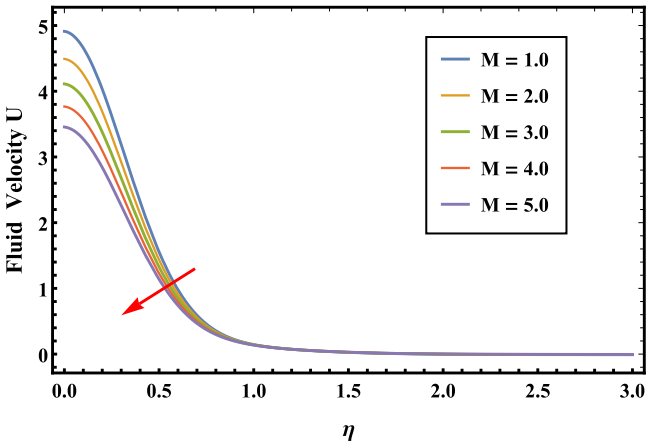

Fig. 2. (Color online) Velocity of fluid for the various values of M.

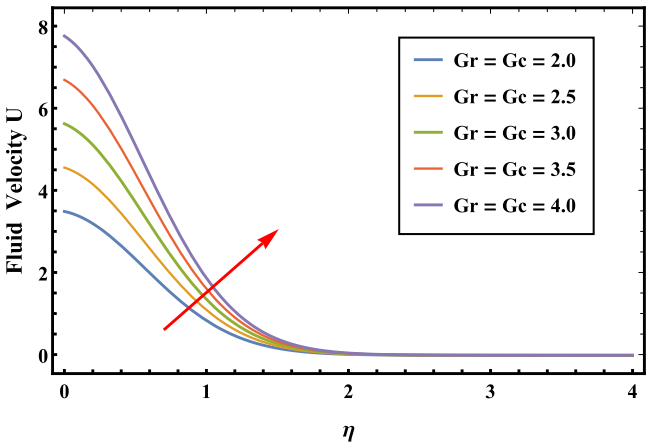

Fig. 3. (Color online) Velocity of fluid for the various values of Gr and Gc.

DOI: 10.1142/S2737416523400100
J. Comput. Biophys. Chem. 2023, 22 (3), 361–370

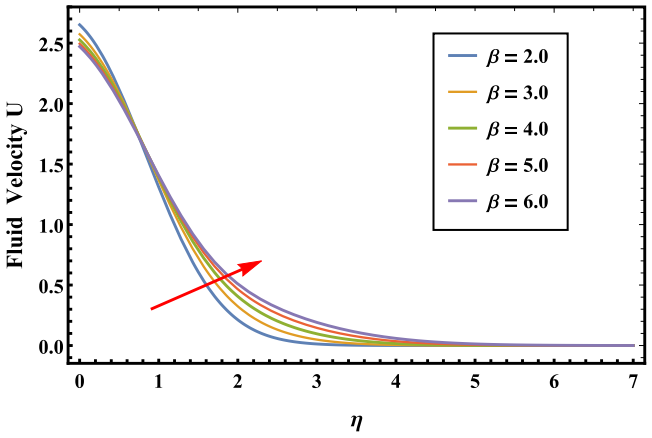

Fig. 4. (Color online) Velocity of fluid for the various values of β.

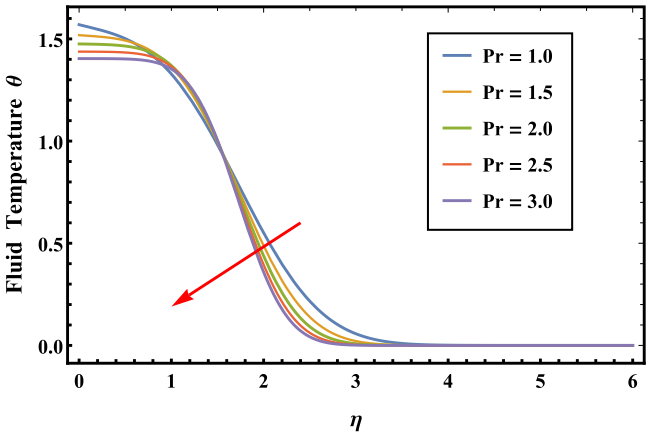

Fig. 6. (Color online) Temperature of fluid for the various values of Pr.

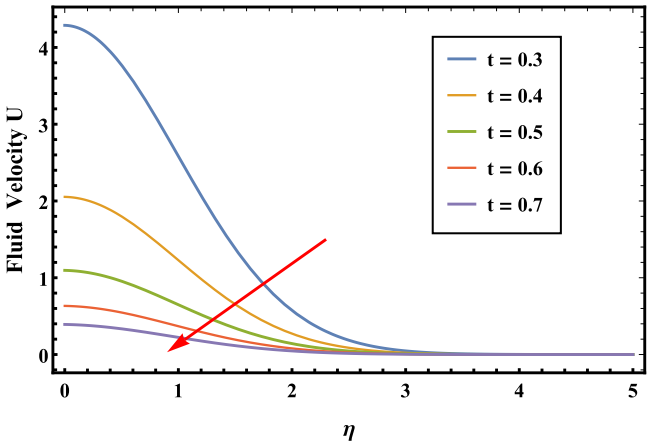

Fig. 5. (Color online) Velocity of fluid for the various values of t.

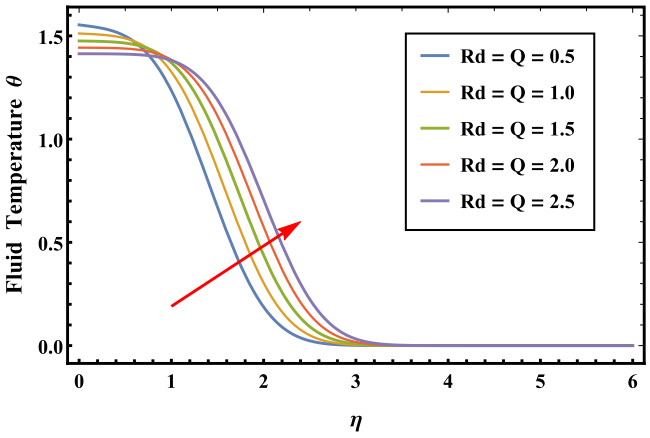

Fig. 7. (Color online) Temperature of fluid for the various values of Rd and Q.

profile vs the Prandtl number by looking at Fig. 6. The Prandtl number is a measure that compares the momentum diffusivity to the thermal diffusivity. An increase in the Prandtl number indicates that a decrease in fluid temperature has occurred due to a higher momentum diffusivity. This fact makes it abundantly clear that the temperature of the fluid is unquestionably increasing as a direct result of the expanding influence of thermal diffusivity throughout the boundary layer region.

As seen in Fig. 7, the temperature profiles rise with an increase in thermal radiation and heat sink parameters. Furthermore, given that one of the effects of the radiation parameter and heat sink is to enhance heat transfer, the thickness of the thermal boundary layer rises with an increase in the amount of thermal radiation and heat sink parameter. Figure 8 illustrates the effect of the Schmidt number on the concentration value. The conclusion that can be drawn from this figure is that greater values of Sc result in a decrease in both fluid concentration and the layer thickness that it is related to. The ratio of momentum diffusivity to heat diffusivity is called the Schmidt number. Momentum diffusivity increases with increasing values of Sc. Because of this, fluid concentration is feeling down in the dumps. Figure 9 depicts the impact of time over concentration fluid. It can be seen from the figure that the concentration boosts with larger values of t.

Figures 10 and 11 describe the variations in the skin friction and Nusselt number for the multiple values of M and Rd against t. Skin friction exhibits upsurging

DOI: 10.1142/S2737416523400100
J. Comput. Biophys. Chem. **2023**, *22* (3), 361–370

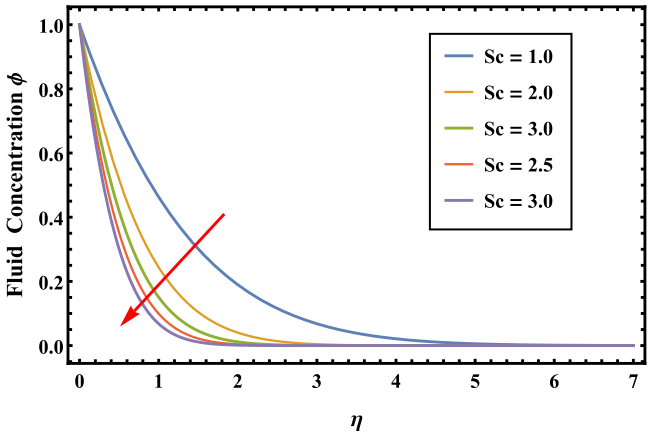

Fig. 8. (Color online) Concentration of fluid for the various values of Sc.

values of behavior through M. It shows that the estimations of Nusselt augment for larger Rd.

In the end, Figs. 12–14 sketch the streamline for the various values of Gr, Gc, M and t. In Table 1, the many possible combinations of the values for the parameters Gr, Gc, M, t and β are compared to their corresponding numerical values for the skin friction. An enhancement in the importance of Gr, Gc, M and β augments skin friction, whereas there is deprecation in skin friction with larger values of t.

Table 2 views the effect of various matters of Rd, Pr, t and Q on Nusselt number. It is examined that the Nusselt number is enhanced with larger values of Rd, Pr, t and Q. Table 3 looks at various values of Sc and t on the Sherwood number. As for the rising importance of Sc and t, obtaining a higher in Sherwood number.

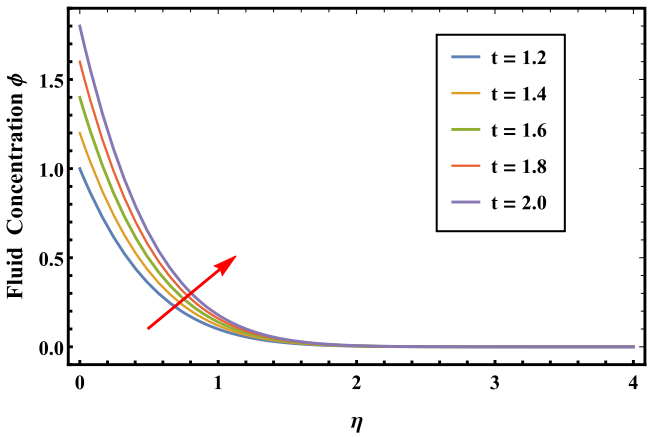

Fig. 9. (Color online) Concentration of fluid for the various values of t.

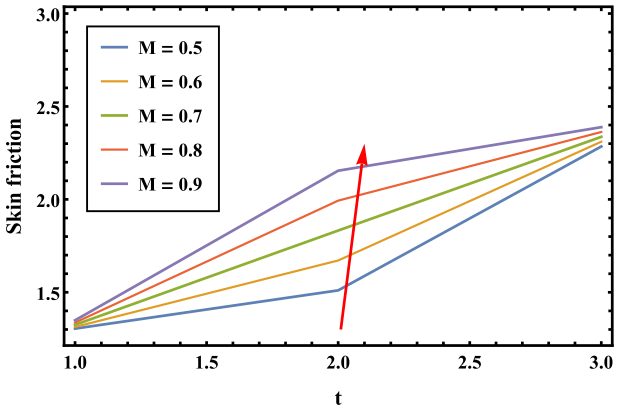

Fig. 10. (Color online) Skin friction of fluid for the various values of M against t.

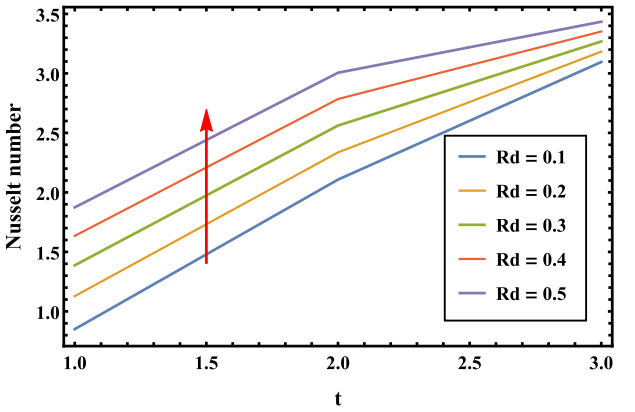

Fig. 11. (Color online) Nusselt number of fluid for the various values of Rd against t.

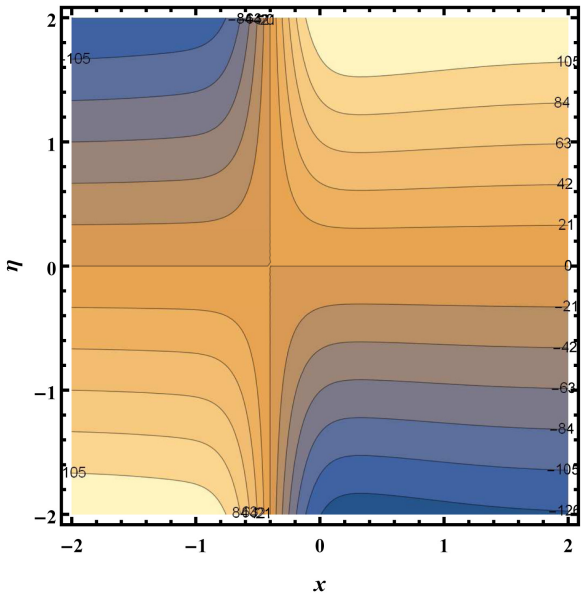

Fig. 12. (Color online) Stream for the $M = 1.0$.

DOI: 10.1142/S2737416523400100
J. Comput. Biophys. Chem. 2023, 22 (3), 361–370

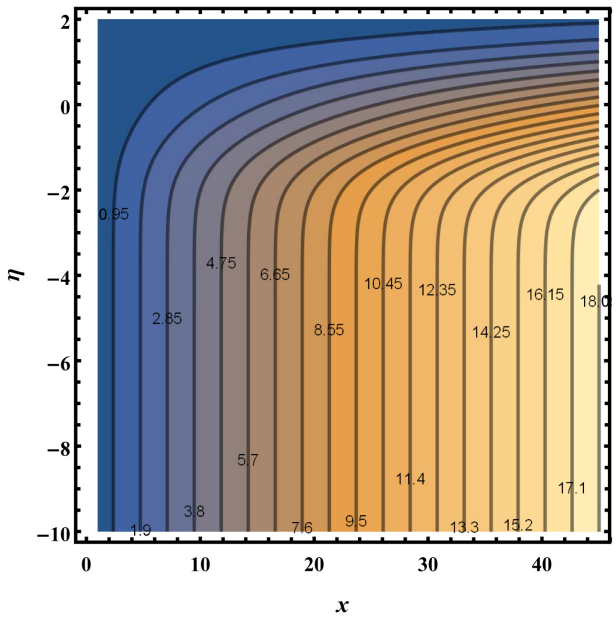

Fig. 13. (Color online) Stream for the $\mathrm{Gr} = \mathrm{Gc} = 1.0$.

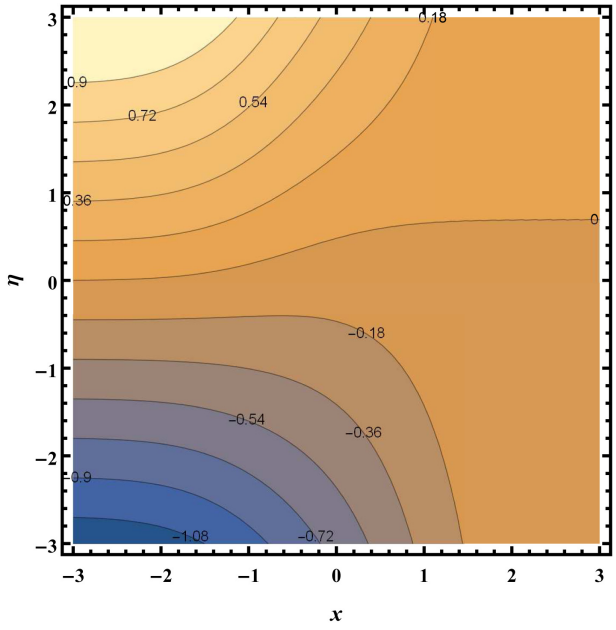

Fig. 14. (Color online) Stream for the β.

4. FINAL REMARKS

This study provides approximate analytical solutions for the motion of Casson fluids over a porous subject to the effects of MHD and mixed convection. We have achieved approximative analytical solutions for the nondimensional velocity field, temperature profile, and concentration distribution in the converted domain by employing the Laplace transform. The impact of the hidden parameters on the fluid velocity field, fluid temperature profile, and fluid concentration distribution has been depicted graphically.

The following is an impression left on these charts:

- Magnetic field declines the fluid velocity.
- Fluid velocity accelerates with rising values of the Casson fluid parameter.
- Thermal Grashof and mass Grashof uplift the fluid velocity.
- As the Prandtl number increases, the fluid temperature distribution decreases.
- Increase in Sc reduces fluid concentration.
- According to Table 1, skin friction enhances both the Casson fluid parameter and the magnetic parameter.

FUNDING INFORMATION

We have no any funding source.

CONFLICT OF INTEREST

All authors have no conflict of interest.

APPENDIX A

If $\alpha = \mathrm{Rd} + Q$, $\eta = \frac{y}{2\sqrt{t}}$, $(1 + \frac{1}{\beta}) = \beta_\circ$, $\epsilon = \beta_\circ \mathrm{Pr} - 1$, $\epsilon_1 = \alpha\beta_\circ - M$ then Skin friction, Nusselt number and Sherwood number are given by

$$\begin{aligned} Cf &= \left[\frac{\partial U}{\partial y}\right]_{y=0} \\ &= \left[\frac{\partial U}{\partial \eta}\right]_{\eta=0} \\ &= \frac{e^{-4Mt}\mathrm{Gc}t^2\beta}{\sqrt{\pi}(\mathrm{Sc}-1)} \\ &\quad + \mathrm{Gr}\gamma_1\left(-\frac{1}{\sqrt{\pi}\epsilon^2}\left(4e^{-\sqrt{\mathrm{Pr}(Q+\mathrm{Rd})}-\mathrm{Pr}(Q+\mathrm{Rd})t}\right)\right. \\ &\quad -\frac{1}{\epsilon^2}\left(-\frac{4e^{-4(Q+\mathrm{Rd})t^2}\sqrt{\mathrm{Pr}(Q+\mathrm{Rd})t}}{\sqrt{\pi}}\right. \\ &\quad \left.\left.-\frac{4e^{-(Q+\mathrm{Rd})t^2}\sqrt{\mathrm{Pr}(Q+\mathrm{Rd})t}}{\sqrt{\pi}}\right)\right), \end{aligned} \tag{A.1}$$

$$\mathrm{Nu} = \left[\frac{\partial\theta}{\partial y}\right]_{y=0} = \left[\frac{\partial\theta}{\partial\eta}\right]_{\eta=0} = -\frac{e^{-4t^2\alpha}\sqrt{\mathrm{Pr}}t^2}{\sqrt{\pi}}, \quad (A.2)$$

$$\mathrm{Nu} = \left[\frac{\partial\phi}{\partial y}\right]_{y=0} = \left[\frac{\partial\phi}{\partial\eta}\right]_{\eta=0} = -\frac{4\sqrt{\mathrm{Sc}}t}{\sqrt{\pi}}. \quad (A.3)$$

References

1. Khan, M. I.; Hayat, T.; Afzal, S.; Khan, M. I.; Alsaedi, A. Theoretical and Numerical Investigation of Carreau–Yasuda Fluid Flow Subject to Soret and Dufour Effects. *Comput. Methods Programs Biomed.* **2020**, *186*, 105145.
2. Raza, A.; Khan, S. U.; Farid, S.; Khan, M. I.; Sun, T. C.; Abbasi, A.; Imran, M.; Malik, M. Thermal Activity of Conventional Casson Nanoparticles with Ramped Temperature Due to an Infinite Vertical Plate Via Fractional Derivative Approach. *Case Stud. Therm. Eng.* **2021**, *27*, 101191.
3. Khan, M. I.; Hayat, T.; Qayyum, S.; Khan, M. I.; Alsaedi, A. Chemically Reactive Flow of Upper-Convected Maxwell Fluid with Cattaneo–Christov Heat Flux Model. *Phys. Lett. A* **2018**, *382*, 2343–2353.
4. Khan, M. I.; Waqas, M.; Hayat, T.; Khan, M. I.; Alsaedi, A. Entropy Generation (Irreversibility) Associated with Flow and Heat Transport Mechanism in Sisko Nanomaterial. *J. Braz. Soc. Mech. Sci. Eng.* **2022**, *39*, 4571–4578.
5. Nazeer, M.; Hussain, F.; Khan, M. I.; Khalid, K. Theoretical Analysis of Electrical Double Layer Effects on the Multiphase Flow of Jeffrey Fluid Through a Divergent Channel with Lubricated Walls. *Waves Random Motion Complex Media* **2022**, *39*.
6. Omar, B. T.; Raghunath, K.; Ali, F.; Khalid, M.; Tag-ElDin, M.; Oreijah, M.; Guedri, K.; Khedher, N. B.; Khan, M. I. Hall Current and Soret Effects on Unsteady MHD Rotating Flow of Second-Grade Fluid Through Porous Media Under the Influences of Thermal Radiation and Chemical Reactions. *Catalysts* **2022**, *12*.
7. Ahmed, M. F.; Zaib, A.; Ali, F.; Omar, B. T.; Tag-ElDin, M.; Guedri, K.; Elattar, S.; Khan, M. I. Numerical Computation for Gyrotactic Microorganisms in MHD Radiative Eyring–Powell Nanomaterial Flow by a Static/Moving Wedge with Darcy–Forchheimer Relation. *Micromachines* **2022**, *13*.
8. Mustafa, M.; Hayat, T.; Pop, I.; Aziz, A. Unsteady Boundary Layer Flow of a Casson Fluid Due to an Impulsively Started Moving Flat Plate. *Heat Transf.-Asian Res.* **2011**, *40*, 563–576.
9. Bhattacharyya, K. MHD Stagnation-Point Flow of Casson Fluid and Heat Transfer Over a Stretching Sheet with Thermal Radiation. *J. Thermodyn.* **2013**, *2013*, 169674.
10. Mukhopadhyay, S.; De, P. R.; Bhattacharyya, K.; Layek, G. C. Casson Fluid Flow Over an Unsteady Stretching Surface. *Ain Shams Eng. J.* **2013**, *4*, 933–938.
11. Nadeem, S.; Haq, R. U.; Lee, C. MHD Flow of a Casson Fluid Over an Exponentially Shrinking Sheet. *Sci. Iran* **2012**, *19*, 1550–1553.
12. Vijaya, K.; Reddy, G. V. R. Magneto Hydrodynamic Casson Fluid Flow Over a Vertical Porous Plate in the Presence of Radiation, Soret and Chemical Reaction Effects. *J. Nanofluids* **2019**, *8*, 1240–1248.
13. Santoshi, P. N.; Reddy, G. V. R.; Reddy, M. G.; Padma, P. Heat and Mass Transfer of Non-Newtonian Nanofluid Flow Over a Stretching Sheet with Non-Uniform Heat Source and Variable Viscosity. *J. Nanofluids* **2018**, *7*, 821–832.
14. Gupta, A. S.; Pop, I.; Soundalgekar, V. M. Free Convection Effects on the Flow Past an Accelerated Vertical Plate in an Incompressible Dissipative Fluid. *Rev. Roum. Sci. Techn.-Mec. Apl.* **1979**, *24*, 561–568.
15. Muthucumaraswamy, R.; Raj, M. S.; Subramanian, V. S. A. Magnetic Field Effects on Flow Past an Accelerated Isothermal Vertical Plate with Heat and Mass Diffusion. *Ann. Fac. Eng. Hunedoara* **2012**, *10*, 177–180.
16. Kafousias, N. G.; Raptis, A. A. Mass Transfer and Free Convection Effects on the Flow Past an Accelerated Vertical Infinite Plate with Variable Suction or Injection. *Rev. Roum. Sci. Techn.-Mec. Apl.* **1981**, *26*, 11–22.
17. Raptis, A.; Singh, A. K. Magnetic Field Effects on Flow Past an Accelerated Isothermal Vertical Plate with Heat and Mass Diffusion. *Int. Commun. Heat Mass Transf.* **1983**, *10*, 313–321.
18. Dhanalakshmi, M.; Jyothi, V.; Reddy, K. J. Soret and Dufour Effects on MHD Convective Flow Past a Vertical Plate Through Porous Medium. *J. Phys., Conf. Ser.* **2019**, *1344*, 012008.
19. Kallepalli, N. S.; Rajasekhar, K.; Ramana, C. V. Influence of Critical Parameters on an Unsteady State MHD Flow in a Porous Channel with Exponentially Decreasing Suction. *J. Math. Comput. Sci.* **2019**, *9*, 764–783.
20. Dharmaiah, G.; Rani, C. B.; Vedavathi, N.; Balamurugan, K. S. Heat and Mass Transfer on MHD Fluid Flow Over a Semi Infinite Flat Plate with Radiation Absorption, Heat Source and Diffusion Thermo Effect. *Front. Heat Mass Transf.* **2018**, *11*, 1–8.
21. Sivaiah, G.; Reddy, K. J.; Reddy, P. C.; Raju, M. C. Numerical Study of MHD Boundary Layer Flow of a Viscoelastic and Dissipative Fluid Past a Porous Plate in

DOI: 10.1142/S2737416523400100
J. Comput. Biophys. Chem. **2023**, *22* (3), 361–370

the Presence of Thermal Radiation. *Int. J. Fluid Mech. Res.* **2019**, *46*, 27–38.
22. Reddy, G. V. R.; Krishna, Y. H. Soret and Dufour Effects on MHD Micropolar Fluid Flow Over a Linearly Stretching Sheet, Through a Non-Darcy Porous Medium. *Int. J. Appl. Mech. Eng.* **2018**, *23*, 485–502.
23. Sujatha, T.; Reddy, K. J.; Kumar, J. G. Chemical Reaction Effect on Nonlinear Radiative MHD Nanofluid Flow Over Cone and Wedge. *Defect Diffus.* **2019**, *393*, 83–102.
24. Ibrahim, S. M.; Mabood, F.; Suneetha, K.; Lorenzini, G. Effects of Chemical Reaction on Combined Heat and Mass Transfer by Laminar Mixed Convection Flow from Vertical Surface with Induced Magnetic Field and Radiation. *J. Eng. Thermophys.* **2017**, *26*, 234–255.
25. Kumar, G. C.; Reddy, K. J.; Ramakrishna, K.; Reddy, M. N. Non-Uniform Heat Source/Sink and Joule Heating Effects on Chemically Radiative MHD Mixed Convective Flow of Micropolar Fluid Over a Stretching Sheet in Porous Medium. *Defect Diffus.* **2018**, *388*, 281–302.
26. Padmavathi, T.; Senthamilselvi, S.; Balasundaram, H.; Makinde, D.; Fernandez-Gamiz, U.; Noeiaghdam, S.; Santra, S.; Altanji, M. Mass Transfer Effects on Mucus Fluid in the Presence of Chemical Reaction. *Alex. Eng. J.* **2023**, *62*, 193–210.
27. Padmavathi, T.; Senthamilselvi, S.; Santra, S. S.; Ali, R.; Govindan, V.; Noeiaghdam, S.; Nieto, J. J. Free and Forced Convective Flow in Pleural Fluid with Effect of Injection Between Different Permeable Regions. *Coatings* **2021**, *11*, 1313.
28. Padmavathi, T.; Senthamilselvi, S.; Karuppusamy, L.; Oluwole, D. M.; Sarris, I. E. Mass Transfer Effects on the Mucus Fluid with Pulsatile Flow Influence of the Electromagnetic Field. *Inventions* **2022**, *7*, 50.
29. Padmavathi, T.; Senthamilselvi, S.; Santra, S. S.; Govindan, V.; Altanji, M.; Noeiaghdam, S. Rotational Reaction Over Infected Covid19 on Human Respiratory Tract in the Presence of Soret Effect with Hall Current. *Bull. Irkutsk State Univ. Ser. Math.* **2022**, *40*, 15–33.
30. Padmavathi, T.; Senthamilselvi, S.; Santra, S. S.; Govindan, V.; Altanji, M.; Noeiaghdam, S. Natural Convection on Pleural Fluid Flow with Applied Magnetic Field Over Covid-19. *J. Algebr. Stat.* **2022**, *13*, 4309–4316.

DOI: 10.1142/S2737416523400100